Skyrmions Under Control—FIB Irradiation as a Versatile Tool for Skyrmion Circuits

Valentin Ahrens, Clara Kiesselbach, Luca Gnoli, Domenico Giuliano, Simon Mendisch, Martina Kiechle, Fabrizio Riente, and Markus Becherer*

Magnetic data storage and processing offer certain advances over conventional technologies, amongst which nonvolatility and low power operation are the most outstanding ones. Skyrmions are a promising candidate as a magnetic data carrier. However, the sputtering of skyrmion films and the control of the skyrmion nucleation, motion, and annihilation remains challenging. This work demonstrates that using optimized focused ion beam irradiation and annealing protocols enables the skyrmion phase in W/CoFeB/MgO thin films to be accessed easily. By analyzing ion-beam-engineered skyrmion hosting wires, excited by sub-100 ns current pulses, possibilities to control skyrmion nucleation, guide their motion, and control their annihilation unfold. Overall, the key elements needed to develop extensive skyrmion networks are presented.

1. Introduction

Skyrmions, magnetic bubbles with a fixed chirality and a topological charge of ±1,[1,2] have been found in several material systems such as noncentrosymmetric ferromagnetic compounds[3,4] van der Waals ferromagnets,[5,6] and sputtered thin films.[7,8] Numerous proposals have been made using skyrmionsas a data carrier in Boolean or new, alternative computing systems.[9–13] However, the number of experimental realizations of these systems is still lacking behind. Reasons for this are the delicate interplay of magnetic energies which stabilizes skyrmions and the difficulties in controlling their nucleation, motion, and annihilation. Sputtered thin films, comprised of a heavy metal layer, a magnetic layer and another heavy metal layer or an oxide, are prospective candidates to host skyrmions. Herein, the magnetic properties of the stack are easily tuned via the individual layer materials and thicknesses. One

typical approach to produce samples with stable skyrmions is the sputtering of wedges, thus scanning a large part of the parameter space by realizing all possible thickness combinations in a certain range.[14–16] Whilst being straightforward and extremely useful for scientific purposes, the small area that actually shows skyrmions and the inherent energy gradient found within this area, are serious obstacles for the development of extensive skyrmion networks. However, not only the materials but also annealing, ion and electron beam irradiation can drastically alter the magnetic properties of thin-film systems.[17–23] Irradiation has already been successfully employed to localize skyrmion appearance in magnetic media.[24,25] Irradiation techniques enable the patterning of magnetic media on the nanometer scale and thus circumvent the highly complex physical structuring in this size range. In this work, we give a detailed description, how skyrmion phases in the archetypal SOT-MRAM system W/CoFeB/MgO[26] can be accessed either via aimed annealing, ion irradiation, or a combination of both. Furthermore, we show that bidirectional (increasing and decreasing) anisotropy manipulation using ion irradiation is possible in this material system. Finally, we demonstrate skyrmion repulsing areas, realized by a drastic reduction of the local anisotropy. From there on, we systematically explore the possibilities of controlling the motion of the skyrmions using these repulsive barriers. We stop, guide, and even nucleate skyrmions in a controlled manner by electrical pulses using different geometries of ion irradiation. While only scratching at the surface of the possibilities of irradiation-controlled skyrmion motion, we demonstrate an essential set of basic building blocks to be used in anticipated skyrmion logic circuits. In contrast to previous works[24,27,28] we use strong ion irradiation to form barriers instead of increasing the skyrmion stability locally. Thus we show an utterly novel approach to tackle the problems on the road toward skyrmion-based devices.

V. Ahrens, C. Kiesselbach, S. Mendisch, M. Kiechle, M. Becherer
Department of Electrical and Computer Engineering
Technical University of Munich
85748 Garching, Germany
E-mail: markus.becherer@tum.de
L. Gnoli, D. Giuliano, F. Riente
Department of Electronics and Telecommunications
Politecnico di Torino
Torino 10129, Italy

2. Results and Discussion

2.1. Film-Level Study

The first goal of this work was the analysis of the effects of Ga+ irradiation on the magnetic layers. To do so, we use a sample that was previously annealed for 10 min at 275 °C in an N2 atmosphere, just sufficient to gain perpendicular

ADVANCED
SCIENCE NEWS
www.advancedsciencenews.com
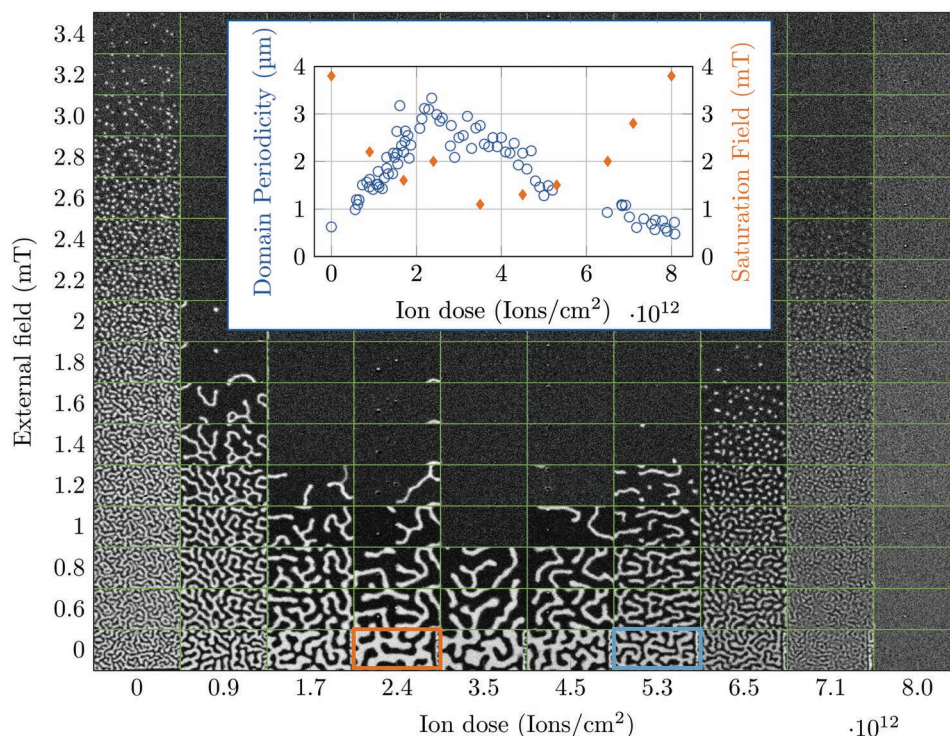
ADVANCED
MATERIALS
www.advmat.de

Figure 1. Magnetic phase diagram of domain structures in Ga$^+$-ion-irradiated parts of the sample, treated with different ion doses as given on the x-axis for each column of images. The rows show the same parts of the sample at different external fields applied in the oop direction given on the y-axis for each row. In the inset plot, the domain periodicity at zero field (last row of the image) is plotted for numerous irradiation doses (blue) giving a comprehensive overview. In the same plot also the magnetic saturation field is shown (orange). The orange and blue squares indicate the closest state to that used in the later studies of the article.

magnetic anisotropy (PMA). In the following, we analyze the domain structure in the annealed film and in squares (20 µm × 20 µm) treated with ion irradiation in fine steps from 8×10^{11} to 1×10^{13} ions cm^{-2}. In **Figure 1**, we present an overview of the domain structure evolution with an increasing external magnetic field (from 0 to 3.4 mT) on the y-axis, and the ion dose on the x-axis. From the pristine domain configuration at zero field (bottom row), an initial increase of the domain size with low irradiation doses is visible. At a turning point, around 2.5×10^{12} ions cm^{-2}, this trend reverses, and we observe a shrinking of the domains. Analyzing the zero-field domain periodicity in fine steps using 2D fast-Fourier-transformation analysis[29] (inset plot Figure 1) reveals the very behavior quantitatively, underlining the rich effects of the ion irradiation on the energy landscape. Furthermore, the saturation field underlines the same development. An increasing irradiation first reduces the magnetic field needed to completely reverse the magnetization in the irradiated square for low doses, while it starts to increase the saturation field again above 3.5×10^{12} ions cm^{-2}. Similar trends have been shown in Ta/CoFeB/MgO thin films[19,30,31] and are attributed to a steep initial increase of the effective anisotropy K_{eff}, caused by a reduction of the saturation magnetization, followed by a gradual decline.

Adding an external magnetic field H_{ext} in the out of plane (oop) direction, as another degree of freedom, allows us to further explore the magnetic phase diagram. In the pristine sample, the domains start to rip apart into individual skyrmions with increasing field. Above around 2 mT only very few

domains remain, after most have transformed into skyrmions. Increasing the external field beyond 2 mT, leads to a reduction of the skyrmion density.

When the sample is further irradiated up to a dose of 4.5×10^{12} ions cm^{-2} no skyrmions are formed, with one exception. A single skyrmion appears at a dose of 0.9×10^{12} ions cm^{-2}, that, however, can be assumed to occur at a larger defect. Furthermore, we observe that the first apparent shrinking of the domains, and their complete annihilation, occurs for intermediate ion doses at lower magnetic fields. The shrinking of the domains at lower magnetic fields is attributed to a reduced pinning potential for irradiated films.[18,32] Beyond that a reduction of the saturation magnetization that in turn leads to weaker demagnetizing fields is expected.[30,32] This effect along with a higher domain wall energy density σ_{DW} in areas with increased effective anisotropy makes a multi-domain-state, energy wise, less favorable compared to a single-domain configuration, and thus lets the domains annihilate at lower external fields.

Beyond an ion dose of 4.5×10^{12} ions cm^{-2} we again observe the formation of a few individual skyrmions at low magnetic fields. The skyrmion density increases for higher ion doses, at the same time the stability against external magnetic fields increases again. For very high ion doses, finally, no domain patterns could be observed. This may be due to our system's limited optical resolution or the transition from an easy-axis to an easy-plane anisotropy with increasing irradiation. Assuming a very low effective anisotropy for the untreated film and at higher doses, our observations are in line with the expectation
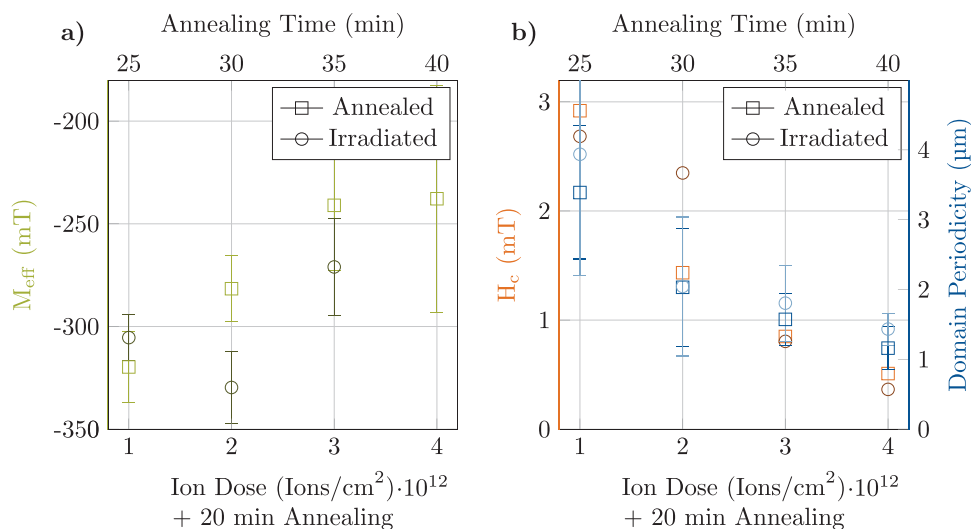
Figure 2. Comparison of the effects of thermal annealing at 275 °C in N_2 atmosphere (squares) and ion irradiation (dots) on a W/CoFeB/MgO sample, by means of FMR and magneto-optical measurements. On the *x*-axis, the respective annealing time (above, starting at 25 min, as the sample was preannealed for 20 min) and ion dose (below) are given. a) The effective magnetization M_{eff} is shown as extracted from the FMR measurements along with its 95% confidence interval of the fit. b) Magneto-optical measurements are used to gain the coercivity H_c and the mean domain periodicity, the error bars are the FWHM of the Gaussian fit.

that bubble formation appears near the spin reorientation transition.[33] Bubble formation in combination with a significant Dzyaloshinskii–Moriya interaction (DMI) consequently leads to the formation of skyrmions.[34,35]

To figure out the effects of the irradiation and compare them to the effects of annealing in **Figure 2**, we used another sample with nominally the same stack. The sample was cut into two pieces to ensure the same starting conditions for both studies. We consider the first steep increase of domain periodicity, as seen in the inset of Figure 1, unsuitable for this study. In this regime, we would be able to collect only few data points, as ion doses far below 1×10^{12} ions cm^{-2} are not reasonably achievable with the used focused ion beam (FIB) system. Therefore the sample was annealed step-wise for 20 min to gain a maximal PMA and access the beginning of the declining part of the domain periodicity graph. The closest state is also marked in Figure 1 by an orange square. From there, the development of both trends of the domain periodicity (dark blue in Figure 2), for thermal annealing (squares) and irradiation (circles) are to a large extent comparable and correlate very well with the periodicity from the inset of Figure 1, assuming the maximum periodicity as a starting point. We see a continuous reduction of the domain periodicity, and the coercive field, while the effective magnetization M_{eff} (which is negative as we are dealing with PMA systems) steadily increases, with increasing irradiation or annealing. An increase of M_{eff}, is often attributed to stronger intermixing of the magnetic layer and an attributed reduction of the saturation magnetization.[23] Beyond the effects on the uniaxial anisotropy and the saturation magnetization, for strong intermixing also a reduction of the effective exchange constant can be considered. Surprisingly, the parameter changes due to irradiation are very similar to that of annealing, within the measurement error range. This correlation gives a strong incidence that also annealing, even in an inert gas atmosphere at such low temperatures as 275 °C, leads to interdiffusion

between the CoFeB layer and the interface materials. Beyond the 3×10^{12} ions cm^{-2} irradiation step and the 40 min annealing step, the SNR in the ferromagnetic resonance (FMR) measurements gets too small to draw based conclusions. This is most likely due to a reduction of the effective, measurable magnetic material that contributes to the signal. Nonetheless, we can clearly state that both annealing and irradiation enable access to similar states of the domain phase diagram.

2.2. Effect of Irradiation on Skyrmions

For now, we have analyzed the effects of ion irradiation on the magnetic properties of the film. As a second step, we evaluate the effects of Ga^+ irradiation on skyrmions. Therefore, we produce a skyrmion hosting sample purely by annealing (state marked in Figure 1 by a blue square). Annealing is used over irradiation as previous studies show that irradiation can drastically alter the skyrmion motion.[24,36] We then analyze the effects of ion irradiation on the size of the skyrmions. We image uniformly irradiated squares (20 µm × 20 µm) magneto-optically and extract the average size of the skyrmions using the spot identification and radius estimation provided by TrackMate,[37] hereby bubbles with low circularity were neglected to reduce the influence of coexisting domains. The skyrmion sizes do not change significantly over a broad range of ion doses, as plotted in **Figure 3**. This invariability does not resemble the increase of the skyrmion size with decreasing anisotropy that are expected from the models of Wang et al.[38] One might argue that the size invariability measured is below the diffraction limit of magneto-optical imaging and therefore is not real. Nonetheless, we see a reduction of the skyrmion size with an increasing external field, throughout the whole ion dose range, which is in line with skyrmion size models[34,38] and experimental observations.[39–41] But, the changes of the skyrmion sizes detected are
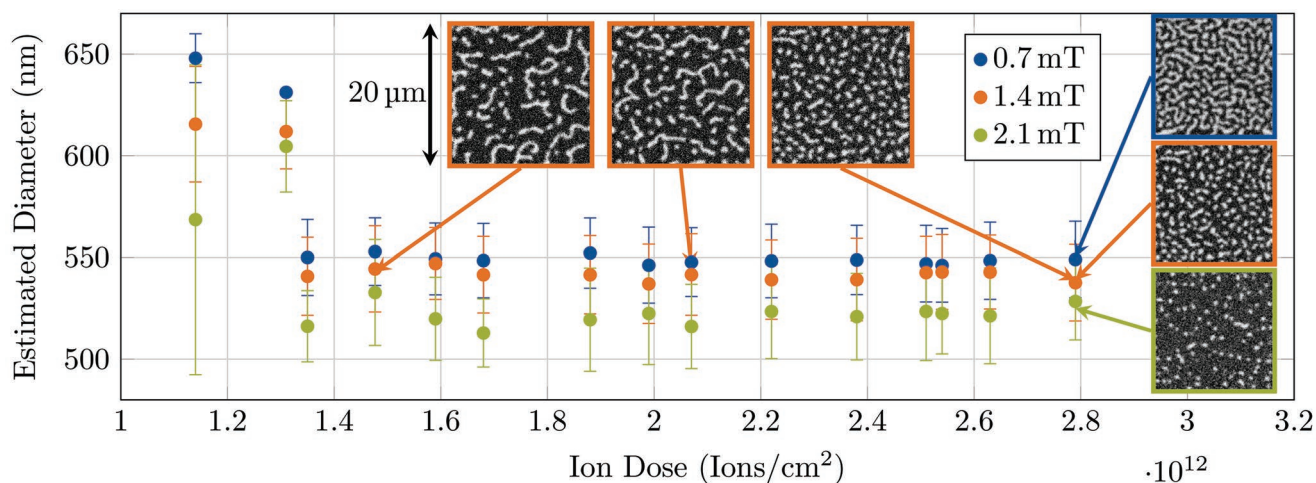
Figure 3. Evaluation of the average skyrmion sizes over the ion dose for three different external magnetic fields. Each data point shows the mean diameter of all skyrmions discovered in the corresponding irradiated areas of the sample (20 μm × 20 μm), and the error bars show the standard deviation of the data. The images in the upper part show the domain structure in these squares for three different ion doses at 1.4 mT. The images on the right present the domain structure for three different external fields and an ion dose of around 2.8×10^{12} ions cm^{-2}.

in the few 10 nm range. Such minimal changes in the skyrmion size are challenging to be detected optically. We argue that due to a large number of skyrmions analyzed we are able to detect even such small changes in the skyrmion size, however we cannot exclude other effects such as the Faraday effect in the objective lens or shifts in the focusing of the microscope to be responsible for the observations. Anyhow, even considering all these additional effects we expect the changes in the average skyrmion size, that can be detected to be below a few 10 nm. The relatively invariant skyrmion size could be explained, assuming that the major contribution to the size change is due to a change of the domain wall width δ_{dw}. Another explanation is that two counteracting mechanisms are occurring at the same time, for example, a reduction of the effective anisotropy K_{eff} along with a reduction of the DMI constant D. This however is considered unlikely as the DMI constant is not expected to be strongly reduced by ion irradiation[18,22] in contrast even an increase of D is possible.[42] Finally the increase of the skyrmion size for low doses even contradicts the skyrmion size models that indicate an increase of the skyrmion size for decreasing anisotropy. The high diameter values for low doses are therefore likely to be measurement artifacts due to the low number of skyrmions in this state, so inevitably more not completely compressed domains are considered. Concluding, we believe that a more detailed investigation of the effects of ion irradiation on skyrmions sizes, by means of higher resolving measurements is needed to shed light on this unexpected behavior.

2.3. From Areal Irradiation to Local Manipulation

Low-dose ion irradiation (1×10^{12} to 4×10^{12} ions cm^{-2} for Ga$^+$, 1×10^{14} to 4×10^{16} ions cm^{-2} for He$^+$) has proven to be a versatile and flexible tool to engineer the magnetic properties and, consequently, the skyrmion motion.[24,28,36]

The concept of creating tracks by irradiating the tracks themselves with ions, as presented in refs. [24, 28], while being

straightforward and working well, potentially comes with the downside of introducing additional pinning centers in the track. The higher number of atomic defects, created by the irradiation, is feared to increase depinning currents and even reduce skyrmion velocities in the track as shown in ref. [36].

Therefore, our aim was to create repulsive barriers for the skyrmions, by strong FIB irradiation, and thus tailor the skyrmions trajectories. For our experiments that scrutinize current-driven skyrmion motion, we decided to use samples that show a large number of skyrmions but still feature them in the isolated state at low fields. The domain state of the sample is shown with a blue square in Figure 1. Here, it is important to mention that, when applying current pulses to the magnetic layers, the number of observed skyrmions significantly increases as domains get ripped apart into skyrmions. Moving the investigated magnetic structures by current also gives us a strong hint that they are actually skyrmions as they move as rigid objects instead of simply expanding (which would be the case for topologically trivial magnetic bubbles). In addition, we clearly see the angular motion due to the skyrmion Hall effect, which further substantiates our assumption. Beyond that, also other publications show stable skyrmions in the same material system,[36,43] however a direct proof of the skyrmion nature (analyzing the DW structure by, e.g., Lorentz TEM) was out of the scope of this work.

2.3.1. Repulsive FIB Barriers

To first prove that the FIB irradiated areas are actually repulsive we treated a magnetic wire locally with a ion dose of 1×10^{13} ions cm^{-2}. With this technique we created tracks of different width ranging from 0.5 to 3 μm by irradiating the surroundings with Ga$^+$ ions. One example, a 0.5 μm-wide track, is shown by the transparent green areas in **Figure 4**a. Below 2 μm track-width, when applying current pulses to push a skyrmion toward the entrance of the small track, the skyrmions cannot
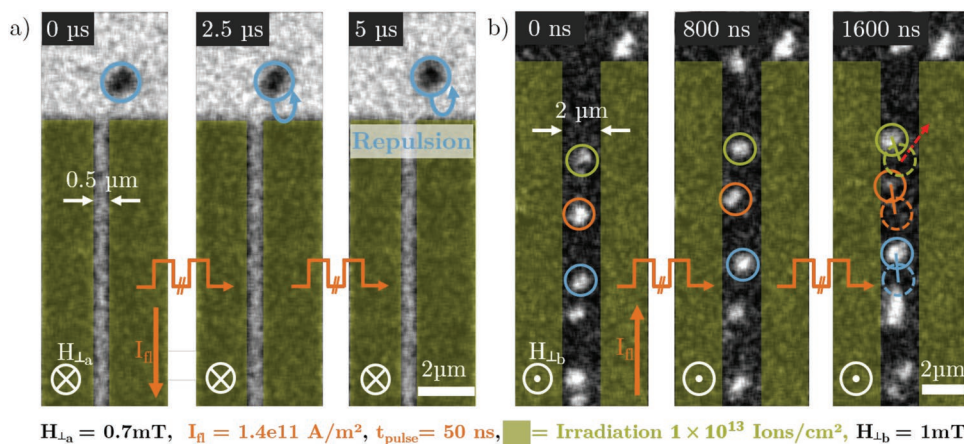
Figure 4. Two series of magneto-optical images of current-driven skyrmions. a) A track, exposed to an oop field of −0.7 mT, that is composed of the untreated magnetic film while the surrounding barriers, indicated in transparent green, are irradiated with an FIB with high ion dose ($\approx 1 \times 10^{13}$ ions cm^{-2}). The same skyrmion after 0, 50 and 100, 50 ns-long current pulses with a current density of 1.4×10^{11} A m^{-2} (cumulative pulse time given in the images), is not able to enter the 500 nm-wide track but is repelled from the irradiated areas. b) Three skyrmions, driven by current pulses (images after 0, 16 and 32, 50 ns-long pulses, current density 1.4×10^{11} A m^{-2}), at a constant perpendicular field of 1 mT. The skyrmions move along a 2 µm-wide track, formed by Ga$^+$ irradiation. The skyrmions move straight along the track as the heavily irradiated areas act as a repulsive barrier, counteracting the motion due to the Magnus force. In the final image, the beginning and end positions of the skyrmions are indicated to visualize the straight motion along with the hypothetical free motion of a skyrmion in red.

enter the track. For our example track from Figure 4a, the skyrmion stays at the same spot even after application of 100, 50 ns-long current pulses with a current density of 1.4×10^{11} A m^{-2}, while the skyrmions in other parts of the film move freely. Increasing the current density now enables the skyrmion to be pushed over the repulsive force into the FIB area, annihilating it in a controlled manner.

The track, too small for the skyrmion to enter, thus creates an effective barrier for the skyrmion and keeps it in one spot. At the same time, skyrmions that nucleate inside of the track are annihilated within a few (below 5) pulses as they immediately touch the walls of the artificial confinement. In literature, the concept of repulsive point defects for skyrmions is well supported, in the form of analytical and numerical calculations[44] and ab initio studies[45] that finds the origin of the repulsive force in the high non-collinearity at the defect site. In ref. [46] a simulative study shows repulsion of skyrmions by areas with strongly reduced anisotropy. This repulsion appears due to the fact that the skyrmions are unstable in the regions with modified anisotropy, thus a repulsive dipolar force guides the skyrmion along that region. Therefore, we assume the irradiated regions to act repulsive on the skyrmions in the same manner. The irradiated regions still maintain a magnetization, but with an easy-plane anisotropy. At the border also local field gradients can occur that are known to influence skyrmion motion as well.[43,47] Alternatively, the irradiated areas can be considered mostly non-ferromagnetic, as a large amount of the magnetic atoms are displaced into the W layer or even the substrate, due to multiple recoil events. Even more, also magnetic atoms that persist in the layer can be oxidized due to the excess oxygen in the MgO in its vicinity. In this case, we would encounter skyrmion edge repulsion[48,49] that follows a similar mechanism as for the areas with strongly reduced anisotropy. One might argue that also a local change of the electric conductivity, induced by the ion irradiation, could lead to a change

in the skyrmion motion. To rule out effects on the resistivity, we analyzed the resistance of four different magnetic wires on the same sample with equal dimensions (30 µm × 35 µm). Two of these wires were untreated, and two had irradiated tracks covering nearly one-fourth of the wire, one with a dose of 5×10^{12} ions cm^{-2} the other with 1×10^{13} ions cm^{-2}, respectively. The resistances of the untreated wires were 468 and 503 Ω while the stronger irradiated wire had a resistivity of 500 Ω and the less irradiated wire of 483 Ω. We do not see any trend in the change of the resistance of the wires with altering irradiation in the used dose range and thus do not expect relevant influences.

2.3.2. Skyrmion Tracks

As we have seen, strongly FIB irradiated areas exert a repulsive force on the skyrmions. To counteract the Magnus force we analyzed wider tracks (2 to 3 µm) in the current direction surrounded by FIB areas. The "free" motion of skyrmions in the untreated film we see is the expected angular motion under the skyrmion Hall angle. In contrast, in the tracks the skyrmions move straight, as they are repelled from the walls. A series of images revealing three skyrmions traveling straight along a 2 µm is presented in Figure 4b. For this track, a mostly linear flow of individual skyrmions is achieved. Also for the 2.5 µm-wide track we see motion of skyrmions along the track, with diminished directionality, meaning that more angular motion from one side of the track to the other is apparent. Nonetheless, the skyrmions move along the track. For the even wider track (3 µm), the amount of nonstraight motion events is further increased. Summing up, we can influence the motion of skyrmions by repulsive barriers in a way that they counteract the effects of the Magnus force, and the skyrmions move straight along tracks and in the direction of the current flow. To
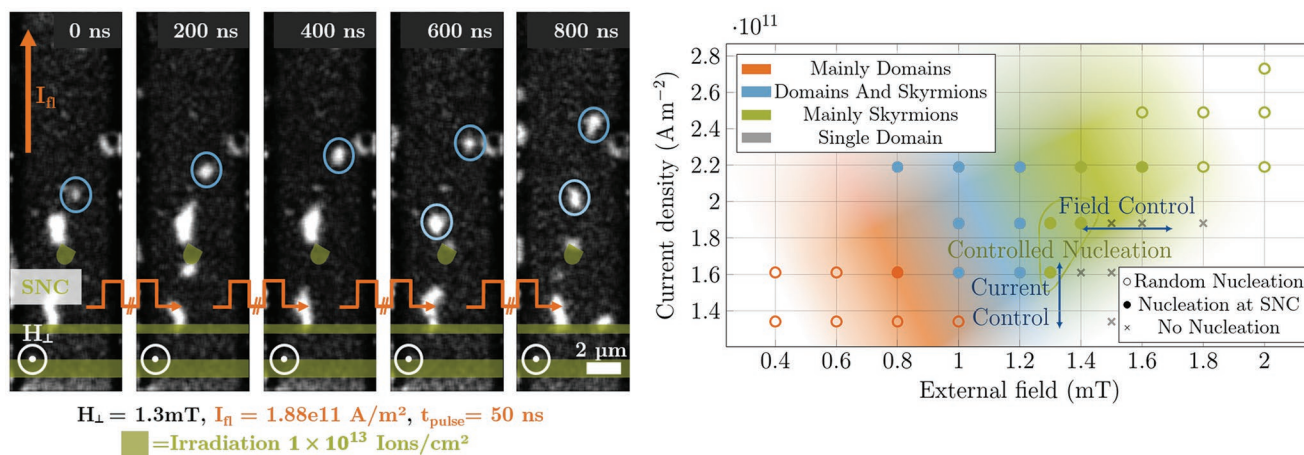
Figure 5. Detailed analysis of the nucleation process of skyrmions and domains at an FIB-created skyrmion nucleation center. a) Series of images showing the consecutive nucleation of two skyrmions (blue circles) at a heavily irradiated SNCs, represented in transparent green. Images are shown after 0, 4, 8, 12, and 16 pulses with a duration of 50 ns and a current density of 1.88×10^{11} A m^{-2}. b) Phase diagram showing an overview of how driving 50 ns current pulses with a given current density (y-axis) at a given external field (x-axis) affect the nucleation at the structure from (a). The marker shape indicates the form of nucleation encountered for the given combination of current and magnetic field. It has to be noted that also in the random nucleation case we still see nucleation at the SNC. The color of the marker, on the other hand, shows the dominant magnetic state for this combination. From low currents and low fields to high currents and high fields, there is a transition from a dominant domain state (orange) over the coexistence of skyrmions and domains (blue) to a prevalence of skyrmions (green). The transparent green region indicates the parameter combinations where controlled nucleation of stable skyrmions is possible.

minimize the effects of Joule heating, we deliberately used low current densities to move the skyrmions, just enough to gain a steady motion. The average skyrmion velocity in the track is with 0.97 m s^{-1} slightly lower than in the free film, where we measure a velocity of 1.50 m s^{-1}. However, considering a skyrmion Hall angle of 35° as shown in other publications,[36,50] we gain a velocity component of the motion in the direction of the current that is with 1.23 m s^{-1} close to what we measured in the free film, while for an irradiated track we would expect to need a higher current density to even achieve a steady motion.[36]

2.3.3. Skyrmion Nucleation Centers

We only miss out on the nucleation device to complete the set of fundamental skyrmion circuit elements, nucleation, guiding, and annihilation. We employed the same irradiation as for guiding and annihilation, for the controlled nucleation of skyrmions. A heavily irradiated skyrmion nucleation center (SNC) is created using a dose of $\approx 1 \times 10^{13}$ ions cm^{-2}. A series of images showing skyrmion nucleation at such an SNC is presented in **Figure 5**a. While we created SNCs with different shapes (circles, drops, and semicircular D-shaped structures), we observed the same behavior for all shapes and used semicircular SNCs for the following studies as visualized in Figure 5a. In contrast to the shape, the size of the SNC can have a drastic influence. At circles with a diameter up to 500 nm we could not detect a relevant change in the nucleation behavior. This means that no SNC can be created with too small structures, this limit is near the size of the skyrmions and therefore most likely scales with the skyrmion size. Structures larger than 2 μm can nucleate skyrmions at different sites, thus becoming unpredictable. Intermediate sized SNCs (1.2 μm diameter) can nucleate individual skyrmions in a deterministic way. The concept of

nucleation of skyrmions at defects with lower anisotropy has already been systematically analyzed using simulations in ref. [51] and observed at natural defects.[52] Although the simulations use structures one order of magnitude smaller than in our experiments, the nucleation process is qualitatively similar. First, a larger domain structure emerges from the irradiated part and finally rips off, forming a skyrmion. But it is important to note that a precise combination of current and magnetic field is needed to nucleate a skyrmion in the wire. Varying both the external magnetic field and the pulse current density, we explored how we can influence the nucleation of skyrmions at the SNC by carefully choosing these parameters. The results of this study, shown in Figure 5b, reveal that the effect of the external magnetic field is very comparable to that observed in Figure 1, meaning that for increasing the external field, we see a transition from a prevalent domain state to a skyrmion state. However, it is worthwhile mentioning that this transition point is shifted toward lower fields for higher current density pulses. In other words, a sufficiently large field can compress the domains right away into skyrmions. Strong current pulses consequently can rip apart domains into smaller ones that in turn can be compressed into skyrmions already by lower fields. While stronger current pulses facilitate nucleation at the SNC, with increasing current, in this case above 2.2×10^{11} A m^{-2}, we start to also see more and more random nucleation of skyrmions throughout the wire. This nucleation is expected to occur due to spin-orbit torque mediated switching.[52] Furthermore, these intense pulses can also randomly annihilate skyrmions by the same mechanism and are thus not suitable for the intended task of controlled nucleation. While the individual switching events are most likely initiated by thermal fluctuations, we expect Joule heating to play a negligible role, due to the short length (50 ns) and the low duty cycle (below 5%) of the current pulsing. Indeed, using the quasi-1D heat transport approach

from ref. [53], we can estimate the steady-state temperature increase in the magnetic wire used for nucleation (resistance of the wire $R_{wire} \approx 1.6$ kΩ) with the given maximum current densities and duty cycle as 6.1 K (details of the estimation are given in Supporting Information). This is, however, neglecting the electrical contacts comprised of 400 nm-thick Cu layers, that additionally act as a heat sink thus further reducing the Joule heating effect. In the central part of the phase diagram, we see the coexistence of skyrmions and domains and a significantly increased probability of nucleation of one or the other at the created SNC. When the parameters are chosen carefully, we can find a window where deterministic nucleation of skyrmions at the SNC is possible, marked with a transparent green background in Figure 5. When we now want to control whether or not a skyrmion is nucleated at the SNC, we have two options. On the one hand, the straightforward solution is to adjust the pulse current to either nucleate a skyrmion or shift it with a lower current but at low velocity. To use this concept, a local separation of the nucleation center and the skyrmion track would be needed. On the other hand also a slight increase of the magnetic field from 1.2 mT and below to 1.3 or 1.4 mT shifts the nucleation from domains toward skyrmions. Increasing the magnetic field further can also completely inhibit the nucleation of new magnetic textures, while keeping the existing skyrmions stable. This paves the way toward a combination of skyrmionic and domain wall based devices where the dipolar fields of a nanomagnet, as used, for example in perpendicular nanomagnetic logic,[30,54] can turn on and off the nucleation of skyrmions, thus writing new skyrmions in a track for one of the two possible coupling fields.

3. Outlook

Concluding, we have proven that targeted annealing and irradiation enables the skyrmion phase to be accessed easily in sputtered thin films. In contrast, the influence of irradiation on the skyrmions size seems low. Furthermore, strong FIB irradiation is a versatile tool to tailor skyrmion motion locally. It enables to build barriers and skyrmion nucleation centers. We mainly focused on the usability of the investigated mechanisms for logic and storage purposes. However, the exact mechanisms behind the observed effects still appear largely unclear. To disentangle the exact interplay between the highly complex effects, supportive simulations and measurements with a much higher lateral and time resolution will be needed. On the other hand, going the next step toward skyrmion-based computing devices represents a steady option. The first step here, is the transition to technologically relevant sub-50 nm skyrmions with sufficient stability over a broad field range. The irradiated structures are typically in the range of the skyrmion size and an irradiation resolution of 20 nm is easily achievable with common FIB systems to manipulate magnetic properties.[55] Therefore, we consider a scaling down to this size range unproblematic, eventually switching to He⁺ ions for even higher precision and smaller structures.

Another material system with smaller, more stable skyrmions also enables building of more complex skyrmion networks. In such, more robust, systems we also expect the random nucleation due to stronger current pulses to be considerably reduced. Potential candidates are multilayers of the same material stack,[43] low damping CoFe based thin films with stable skyrmions over a broad field range,[56] or antiferromagnetically coupled bilayers that show highly stable skyrmions at zero field.[57] Nonetheless, the ability to build tracks in nearly arbitrary shapes with high precision opens doors toward realizing proposed skyrmions logic systems like conservative logic.[9] In this light, it might be worthwhile to further explore the effect of varying ion doses on the nucleation mechanism and the repulsive force acting from the barriers. Going even further, coupling nanomagnets to skyrmion nucleation centers, exploiting the field dependence of the nucleation, logical states can theoretically be transferred from one domain (domain wall logic) to the other (skyrmion logic). Realizing such systems is the next logical step to combine the benefits of both technologies and merge two prospective, beyond complementary metal–oxide–semiconductor (CMOS), spintronic device concepts without leaving the magnetic domain. Finally, also the use of the presented results for reservoir computing,[58] Brownian computing,[59] and other non-Boolean architectures is a thought-provoking approach as it can short pass the intricate physical structuring.

4. Experimental Section

Sample Fabrication: Samples comprised of Si/SiO₂/W(3)/Co₂₀Fe₆₀B₂₀(0.9)/MgO(1)/Ta(1), with the respective layer thickness in nm given in brackets, serve as skyrmion host for the studies. These samples were produced in a home-built RF-sputter deposition system realized in a confocal geometry to enable reasonably short delays between the deposition of the individual layers. After deposition of the layers, the magnetic properties were adjusted using an annealing step in a N₂ atmosphere at 275 °C. The annealed films were covered with another 3 nm layer of Ta to protect them during the subsequent processing steps. Then the samples were structured by optical lithography and ion beam etching (Ar⁺), utilizing a nominally 2 µm-thick photoresist as a hard mask. For current pulsing experiments, another lithography, e-beam deposition, and lift-off step were performed to make contact structures for individual magnetic wires. An exemplary image of a contacted magnetic wire along with an illustration of the measurement setup is shown in **Figure 6**.

Focused Ion Beam Irradiation: To tailor the magnetic properties locally, a 50 keV Ga⁺ focused ion beam system with a nominal beam diameter of 5 nm was used. Aiming for ion doses ranging from below 1×10^{12} to 2×10^{13} ions cm⁻², the ion beam current at 2 pA was fixed and the irradiation time was adjusted to the desired value. The used Micrion 9500 EX FIB system, allowed for irradiation of arbitrary shapes enabling the realization of tracks and spots on the structured magnetic wires. It is worth mentioning that though strong irradiation is spoken of, to separate distinct irradiation regimes in the article, the used ion doses were far from those needed to physically mill the material.[60] While an ion dose of 1×10^{13} ions cm⁻² might appear low, and in fact means that only a single ion per 10 nm² hit the surface of the film, the effect of low dose ion irradiation on the magnetic properties was drastic. Reason for that was the high amount of recoils and secondary collisions in the magnetic film that caused a huge amount of atomic displacements in the material stack. Using Monte Carlo based stopping and range of ions in matter simulations,[61] it is found that each ion caused ≈1000 atomic displacements in a radial range of ≈15 nm around the point of entrance of the Ga⁺ ion. Even more the vast majority of these collisions (per material volume) took place in the Ta and W layers and with a slightly lower ratio in the CoFeB and MgO layers. The underlying SiO₂ and Si layers were significantly less affected.
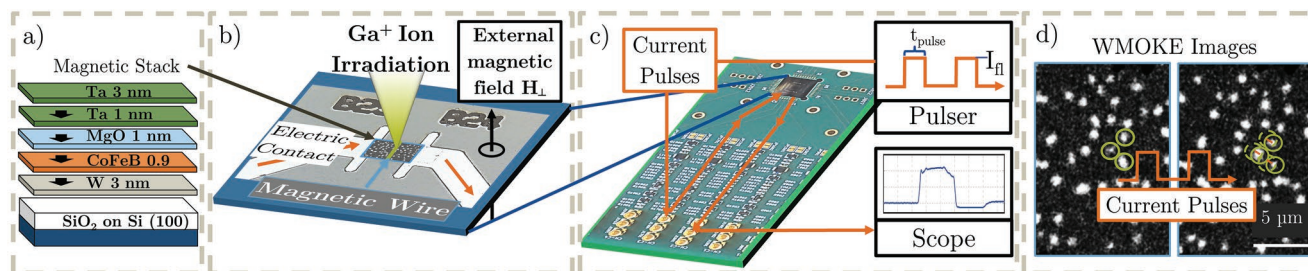
**ADVANCED
SCIENCE NEWS**

www.advancedsciencenews.com

**ADVANCED
MATERIALS**

www.advmat.de

Figure 6. Schematic overview of the employed measurement system. a) Magnetic material stack. b) Structured and electrically contacted magnetic wires, visualizing the concept of local Ga$^+$ ion irradiation on the wires. c) Dedicated chip carrier board that guides the current pulses sent from a nanosecond-pulser, with pulse-width t_{pulse}. Consequently, the pulses are measured via an oscilloscope to extract the exact current densities I_{fl}. d) An exemplary wide-field magneto-optical Kerr effect (WMOKE) measurement where current pulses move the skyrmions in a magnetic wire. By imaging before and after a number of current pulses the skyrmion trajectories are extracted.

Metrology: The magnetic structures were analyzed using magneto-optical measurement systems in laser and wide-field, polar Kerr effect configuration. These measurement systems enabled the recording of hysteresis loops and the imaging of magnetic domains on the samples. Beyond static domain images, recording current-driven skyrmion motion was possible in a quasi-static manner. The skyrmions were imaged in the magnetic wire, current pulses were injected in the nanosecond timescale, and the same wire was imaged again. From the differences in these images, it was possible to track the displacement of the magnetic textures caused by the current pulses. The TrackMate algorithm[37] enabled extraction of velocities and the skyrmion Hall angle. To be able to measure the pulse current precisely, one side of the magnetic wire was connected to the 50 Ω input of a fast oscilloscope, while the other side was connected to a current pulser. In order to assess the current density, the width of the magnetic wire and the thickness of the entire sputtered stack ($t_{stack} \approx 8.9$ nm) minus the thickness of the MgO layer (1 nm) was used. As a result of this, the current that contributes to the motion of the skyrmions but can give an upper bound for the needed current densities was knowingly overestimated.

Supporting Information

Supporting Information is available from the Wiley Online Library or from the author.

Conflict of Interest

The authors declare no conflict of interest.

Data Availability Statement

The data that support the findings of this study are available from the corresponding author upon reasonable request.

Keywords

focused ion beam, magnetic thin-films, skyrmionics, skyrmions, spintronics

[1] A. N. Bogdanov, C. Panagopoulos, *Nat. Rev. Phys.* **2020**, 2, 492.
[2] A. Fert, N. Reyren, V. Cros, *Nat. Rev. Mater.* **2017**, 2, 17031.
[3] N. Kanazawa, S. Seki, Y. Tokura, *Adv. Mater.* **2017**, 29, 1603227.
[4] L. Peng, R. Takagi, W. Koshibae, K. Shibata, K. Nakajima, T.-H. Arima, N. Nagaosa, S. Seki, X. Yu, Y. Tokura, *Nat. Nanotechnol.* **2020**, 15, 181.
[5] Y. Wu, B. Francisco, Z. Chen, W. Wang, Y. Zhang, C. Wan, X. Han, H. Chi, Y. Hou, A. Lodesani, G. Yin, K. Liu, Y.-t. Cui, K. L. Wang, J. S. Moodera, *Adv. Mater.* **2022**, 34, 2110583.
[6] B. Ding, Z. Li, G. Xu, H. Li, Z. Hou, E. Liu, X. Xi, F. Xu, Y. Yao, W. Wang, *Nano Lett.* **2019**, 20, 868.
[7] W. Legrand, D. Maccariello, N. Reyren, K. Garcia, C. Moutafis, C. Moreau-Luchaire, S. Collin, K. Bouzehouane, V. Cros, A. Fert, *Nano Lett.* **2017**, 17, 2703.
[8] G. Yu, P. Upadhyaya, X. Li, W. Li, S. K. Kim, Y. Fan, K. L. Wong, Y. Tserkovnyak, P. K. Amiri, K. L. Wang, *Nano Lett.* **2016**, 16, 1981.
[9] M. Chauwin, X. Hu, F. Garcia-Sanchez, N. Betrabet, A. Paler, C. Moutafis, J. S. Friedman, *Phys. Rev. Appl.* **2019**, 12, 064053.
[10] Y. Huang, W. Kang, X. Zhang, Y. Zhou, W. Zhao, *Nanotechnology* **2017**, 28, 08LT02.
[11] X. Zhang, M. Ezawa, Y. Zhou, *Sci. Rep.* **2015**, 5, 9400.
[12] L. Gnoli, F. Riente, M. Vacca, M. Ruo Roch, M. Graziano, *Electronics* **2021**, 10, 155.
[13] J. Zhou, J. Chen, *Adv. Electron. Mater.* **2021**, 7, 2100465.
[14] T. Srivastava, W. Lim, I. Joumard, S. Auffret, C. Baraduc, H. Béa, *Phys. Rev. B* **2019**, 100, 220401.
[15] J. A. Brock, E. E. Fullerton, *Adv. Mater. Interfaces* **2022**, 9, 2101708.
[16] Q. Yang, Y. Cheng, Y. Li, Z. Zhou, J. Liang, X. Zhao, Z. Hu, R. Peng, H. Yang, M. Liu, *Adv. Electron. Mater.* **2020**, 6, 2000246.
[17] J. Fassbender, J. McCord, *J. Magn. Magn. Mater.* **2008**, 320, 579.
[18] X. Zhao, B. Zhang, N. Vernier, X. Zhang, M. Sall, T. Xing, L. H. Diez, C. Hepburn, L. Wang, G. Durin, A. Casiraghi, M. Belmeguenai, Y. Roussigné, A. Stashkevich, S. M. Chérif, J. Langer, B. Ocker, S. Jaiswal, G. Jakob, M. Kläui, W. Zhao, D. Ravelosona, *Appl. Phys. Lett.* **2019**, 115, 122404.
[19] L. Herrera Diez, F. García-Sánchez, J.-P. Adam, T. Devolder, S. Eimer, M. El Hadri, A. Lamperti, R. Mantovan, B. Ocker, D. Ravelosona, *Appl. Phys. Lett.* **2015**, 107, 032401.

[20] H. Shi, M. Li, S. Fang, W. Zhou, C. Yang, Y. Jiang, D. Wang, G. Yu, *Surf. Interface Anal.* **2018**, *50*, 59.

[21] Y.-H. Wang, W.-C. Chen, S.-Y. Yang, K.-H. Shen, C. Park, M.-J. Kao, M.-J. Tsai, *J. Appl. Phys.* **2006**, *99*, 08M307.

[22] M. C. De Jong, M. J. Meijer, J. Lucassen, J. Van Liempt, H. J. Swagten, B. Koopmans, R. Lavrijsen, *Phys. Rev. B* **2022**, *105*, 064429.

[23] W. Ruane, S. White, J. Brangham, K. Meng, D. Pelekhov, F. Yang, P. Hammel, *AIP Adv.* **2018**, *8*, 056007.

[24] R. Juge, K. Bairagi, K. G. Rana, J. Vogel, M. Sall, D. Mailly, V. T. Pham, Q. Zhang, N. Sisodia, M. Foerster, L. Aballe, M. Belmeguenai, Y. Roussign, S. Auffret, L. D. Buda-Prejbeanu, G. Gaudin, D. Ravelosona, O. Boulle, *Nano Lett.* **2021**, *21*, 2989.

[25] Y. Guang, Y. Peng, Z. Yan, Y. Liu, J. Zhang, X. Zeng, S. Zhang, S. Zhang, D. M. Burn, N. Jaouen, J. Wei, H. Xu, J. Feng, C. Fang, G. van der Laan, T. Hesjedal, B. Cui, X. Zhang, G. Yu, X. Han, *Adv. Mater.* **2020**, *32*, 2003003.

[26] K. Garello, F. Yasin, H. Hody, S. Couet, L. Souriau, S. H. Sharifi, J. Swerts, R. Carpenter, S. Rao, W. Kim, J. Wu, K. K. V. Sethu, M. Pak, N. Jossart, D. Crotti, A. Furnémont, G. S. Kar imec, in *2019 Symp. on VLSI Circuits*, IEEE, Piscataway, NJ, USA **2019**, pp. T194–T195.

[27] K. Fallon, S. Hughes, K. Zeissler, W. Legrand, F. Ajejas, D. Maccariello, S. McFadzean, W. Smith, D. McGrouther, S. Collin, N. Reyren, V. Cros, C. H. Marrows, S. McVitie, *Small* **2020**, *16*, 1907450.

[28] L.-M. Kern, B. Pfau, V. Deinhart, M. Schneider, C. Klose, K. Gerlinger, S. Wittrock, D. Engel, I. Will, C. M. Günther, K. Litzius, S. Wintz, M. Weigand, F. Büttner, S. Eisebitt, *Nano Lett.* **2022**, *106*, 054435.

[29] M. Yamanouchi, A. Jander, P. Dhagat, S. Ikeda, F. Matsukura, H. Ohno, *IEEE Magn. Lett.* **2011**, *2*, 3000304.

[30] S. Mendisch, F. Riente, V. Ahrens, L. Gnoli, M. Haider, M. Opel, M. Kiechle, M. R. Roch, M. Becherer, *Phys. Rev. Appl.* **2021**, *16*, 014039.

[31] T. Devolder, I. Barisic, S. Eimer, K. Garcia, J.-P. Adam, B. Ockert, D. Ravelosona, *J. Appl. Phys.* **2013**, *113*, 203912.

[32] L. H. Diez, M. Voto, A. Casiraghi, M. Belmeguenai, Y. Roussigné, G. Durin, A. Lamperti, R. Mantovan, V. Sluka, V. Jeudy, Y. T. Liu, A. Stashkevich, S. M. Chérif, J. Langer, B. Ocker, L. Lopez-Diaz, D. Ravelosona, *Phys. Rev. B* **2019**, *99*, 054431.

[33] J. Wu, J. Choi, C. Won, Y. Wu, A. Scholl, A. Doran, C. Hwang, Z. Qiu, *Phys. Rev. B* **2009**, *79*, 014429.

[34] S. Rohart, A. Thiaville, *Phys. Rev. B* **2013**, *88*, 184422.

[35] M. Hervé, B. Dupé, R. Lopes, M. Böttcher, M. D. Martins, T. Balashov, L. Gerhard, J. Sinova, W. Wulfhekel, *Nat. Commun.* **2018**, *9*, 1015.

[36] V. Ahrens, L. Gnoli, D. Giuliano, S. Mendisch, M. Kiechle, F. Riente, M. Becherer, *AIP Adv.* **2022**, *12*, 035325.

[37] J.-Y. Tinevez, N. Perry, J. Schindelin, G. M. Hoopes, G. D. Reynolds, E. Laplantine, S. Y. Bednarek, S. L. Shorte, K. W. Eliceiri, *Methods* **2017**, *115*, 80.

[38] X. Wang, H. Yuan, X. Wang, *Commun. Phys.* **2018**, *1*, 31.

[39] A. Soumyanarayanan, M. Raju, A. Gonzalez Oyarce, A. K. Tan, M.-Y. Im, A. Petrović, P. Ho, K. Khoo, M. Tran, C. Gan, F. Ernult, C. Panagopoulos, *Nat. Mater.* **2017**, *16*, 898.

[40] N. Romming, A. Kubetzka, C. Hanneken, K. von Bergmann, R. Wiesendanger, *Phys. Rev. Lett.* **2015**, *114*, 177203.

[41] C. Moreau-Luchaire, C. Moutafis, N. Reyren, J. Sampaio, C. Vaz, N. Van Horne, K. Bouzehouane, K. Garcia, C. Deranlot, P. Warnicke, P. Wohlhüter, J.-M. George, M. Weigand, J. Raabe, V. Cros, A. Fert, *Nat. Nanotechnol.* **2016**, *11*, 444.

[42] H. T. Nembach, E. Jué, K. Poetzger, J. Fassbender, T. J. Silva, J. M. Shaw, *J. Appl. Phys.* **2022**, *131*, 143901.

[43] A. Casiraghi, H. Corte-León, M. Vafaee, F. Garcia-Sanchez, G. Durin, M. Pasquale, G. Jakob, M. Kläui, O. Kazakova, *Commun. Phys.* **2019**, *2*, 145.

[44] J. Müller, A. Rosch, *Phys. Rev. B* **2015**, *91*, 054410.

[45] I. Lima Fernandes, J. Bouaziz, S. Blügel, S. Lounis, *Nat. Commun.* **2018**, *9*, 4395.

[46] P. Upadhyaya, G. Yu, P. K. Amiri, K. L. Wang, *Phys. Rev. B* **2015**, *92*, 134411.

[47] J. Liang, J. Yu, J. Chen, M. Qin, M. Zeng, X. Lu, X. Gao, J.-M. Liu, *New J. Phys.* **2018**, *20*, 053037.

[48] X. Zhang, G. Zhao, H. Fangohr, J. P. Liu, W. Xia, J. Xia, F. Morvan, *Sci. Rep.* **2015**, *5*, 7643.

[49] R. Duine, *Nat. Nanotechnol.* **2013**, *8*, 800.

[50] W. Jiang, X. Zhang, G. Yu, W. Zhang, X. Wang, M. B. Jungfleisch, J. E. Pearson, X. Cheng, O. Heinonen, K. L. Wang, Y. Zhou, A. Hoffmann, S. G. E. te Velthuis, *Nat. Phys.* **2017**, *13*, 162.

[51] K. Everschor-Sitte, M. Sitte, T. Valet, A. Abanov, J. Sinova, *New J. Phys.* **2017**, *19*, 092001.

[52] F. Büttner, I. Lemesh, M. Schneider, B. Pfau, C. M. Günther, P. Hessing, J. Geilhufe, L. Caretta, D. Engel, B. Krüger, J. Viefhaus, S. Eisebitt, G. S. D. Beach, *Nat. Nanotechnol.* **2017**, *12*, 1040.

[53] W. R. Hunter, *IEEE Trans. Electron Devices* **1997**, *44*, 304.

[54] F. Riente, S. Mendisch, L. Gnoli, V. Ahrens, M. R. Roch, M. Becherer, *AIP Adv.* **2020**, *10*, 125229.

[55] S. Breitkreutz, J. Kiermaier, I. Eichwald, X. Ju, G. Csaba, D. Schmitt-Landsiedel, M. Becherer, *IEEE Trans. Magn.* **2012**, *48*, 4336.

[56] L. Flacke, V. Ahrens, S. Mendisch, L. Körber, T. Böttcher, E. Meidinger, M. Yaqoob, M. Müller, L. Liensberger, A. Kákay, M. Becherer, P. Pirro, M. Althammer, S. Geprägs, H. Huebl, R. Gross, M. Weiler, *Phys. Rev. B* **2021**, *104*, L100417.

[57] A. Hrabec, J. Sampaio, M. Belmeguenai, I. Gross, R. Weil, S. M. Chérif, A. Stashkevich, V. Jacques, A. Thiaville, S. Rohart, *Nat. Commun.* **2017**, *8*, 15765.

[58] D. Pinna, G. Bourianoff, K. Everschor-Sitte, *Phys. Rev. Appl.* **2020**, *14*, 054020.

[59] Y. Jibiki, M. Goto, E. Tamura, J. Cho, S. Miki, R. Ishikawa, H. Nomura, T. Srivastava, W. Lim, S. Auffret, C. Baraduc, H. Bea, Y. Suzuki, *Appl. Phys. Lett.* **2020**, *117*, 082402.

[60] R. Hyndman, P. Warin, J. Gierak, J. Ferré, J. Chapman, J. Jamet, V. Mathet, C. Chappert, *J. Appl. Phys.* **2001**, *90*, 3843.

[61] J. F. Ziegler, J. P. Biersack, in *Treatise on Heavy-Ion Science*, Springer, Berlin/Heidelberg, Germany **1985**, pp. 93–129.